AIAA SciTech Forum
4-8 January 2016, San Diego, California, USA
24th AIAA/AHS Adaptive Structures Conference

10.2514/6.2016-1315

Directionally Variable Stiffness to Reduce Actuation Requirement in Airfoil Camber Morphing

Matthew DiPalma[1] Farhan Gandhi[2]

Rotorcraft, Adaptive and Morphing Structures (RAMS) Lab
Department of Mechanical, Aerospace and Nuclear Engineering
Rensselaer Polytechnic Institute, Troy, NY 12180

This paper explores a new design for an airfoil whose chordwise bending stiffness depends on the direction of load. By designing the region aft of the spar to be very stiff under upward load, uncommanded camber deformation under aerodynamic pressure can be minimized. At the same time, a much higher compliance under a reversed load reduces actuation requirement to achieve a desired downward camber deformation. A rigid cantilever extending from the rear of the spar toward the trailing-edge, and flush with the lower skin, is used to realize this goal. Under upward (aerodynamic pressure) load the rigid cantilever engages and its added stiffness minimizes deformation. But under downward (actuation) load, the lower skin breaks contact with the cantilever, and camber deformation can be achieved at low actuation effort. ABAQUS™ finite element simulations were conducted for a variable camber NACA 0012 airfoil. For a cantilever extending over the entire length of the conformable section (between the leading-edge D-spar and the trailing-edge section), the effective stiffness under upward loading was calculated to be 15.43 times the stiffness under downward loading, but the maximum downward camber deformation was limited to 10 deg due to contact between the cantilever and the upper skin. Reducing the cantilever length increased the maximum downward camber deformation achieved but with a smaller increase in stiffness under upward load.

I. Introduction

It is widely appreciated in the aeronautics community that aircraft wing (or helicopter rotor blade) camber variation can result in improved aerodynamic performance over diverse operating conditions. Offering greater efficiency than the operation of discrete control surfaces (like flaps and ailerons), camber variation can be used for redistribution of lift along the wing or rotor blade, for primary flight control, as well as for gust alleviation and aeroelastic stability problems. From the 1980s to early 2000, major government programs invested significant resources to pursue this technology (Refs. 1–4). More recently, NASA proposed a variable camber continuous trailing edge (VCCTE) flap system for control of highly flexible wing structures designed for low-weight and low aerodynamic drag (Ref. 5).

A substantial amount of prior work is available in the literature on camber morphing (see for example, Refs. 6–23), with the specific approach to achieving the trailing-edge camber strongly dependent on the magnitude of the change sought, the frequency, its spanwise variation, and the specific application. Most of the prior work uses some kind of flexible core/substructure in the morphing region of the airfoil (for example, Refs. 17, 18, 21–23), coupled with diverse actuation methods to camber the trailing edge including shape memory alloys (Refs. 6–10), piezoelectric actuators (Refs. 11–16), pneumatic actuators (Ref. 17), and even conventional servomotors (for example, Ref. 18). Some studies have also used post-buckled elements (Ref. 19), skin warping (Ref. 20), and other mechanisms to amplify the camber deformations. Similarly, another area that has been the subject of much attention over the last several years is the design of high-strain capable flexskins that can simultaneously bear aerodynamic loads and satisfy a range of other constraints (Refs. 23–28).

One of the enduring problems that must be faced in camber morphing is the requirement that the morphing airfoil/wing/rotor blade section be simultaneously rigid to minimize uncommanded deformation under aerodynamic load, and at the same time be somewhat compliant to eschew exorbitant actuation force and energy requirement (which in turn translates to actuator size, weight and power costs). While mathematically optimal solutions that seek to simultaneously meet these apparently conflicting objectives have been pursued, the present study takes a more

[1] Undergraduate Research Assistant
[2] Rosalind and John J. Redfern Jr. ’33 Professor of Aerospace Engineering, AIAA Associate Fellow.

innovative conceptual approach for a specific situation, discussed below. With the upper surface of an airfoil aft of the spar under suction and the lower surface under pressure, the tendency of the aerodynamic loads is to camber the airfoil upward (reflex the airfoil). If the camber deflection sought under actuation is always and only downward (for example, to generate high lift over a section of the wing or helicopter rotor blade), it could be tremendously advantageous to design the aft airfoil as a structure with a much higher chordwise bending stiffness in the upward direction (to limit deformation under aerodynamic load) and a substantially reduced chordwise bending stiffness in the downward direction (to reduce actuation force requirement). The current study presents a concept that would produce such a difference in chordwise bending stiffness based on direction of load, and investigates the performance using a finite element analysis.

II. Concept and Analysis

Consider a slender cantilevered beam of length, *L*, flexural stiffness, *EI*, subjected to an upward tip load, *P*. From strength of materials, the tip displacement is known to be:

$$w = \frac{PL^3}{3EI}$$

Now while the upward load continues to act on the beam, a downward tip load, *F (F > P)* is introduced to reverse the deformation of the beam and cause it to bend down. *F* can be expressed as:

$$F = P + P_1$$

where the component *P* negates the upward force and the component P_1 produces the additional downward deformation from the neutral position. The downward deflection, w_1, is:

$$w_1 = \frac{P_1 L^3}{3EI}$$

If the desired downward deflection is $w_1 = \propto w$, it can be shown that $P_1 = \propto P$, and therefore,

$$F = P + \propto P$$

If $\propto = 10$ (a required downward deflection 10 times the deflection under the upward load, *P*), then clearly, the downward force is 11 times larger than the force *P*. While the first term on the right hand side of Eq. 4 is the term required to overcome the upward force, the second term is the component required to overcome structural stiffness to achieve the desired downward deflection.

Now consider the situation where the structural stiffness for downward deformation is reduced by a factor β, the downward deflection would now be:

$$w_1 = \frac{P_1 L^3}{3EI/\beta}$$

If the desired downward deflection is once again $w_1 = \propto w$, then it can be shown that $P_1 = \frac{\propto}{\beta} P$, and therefore,

$$F = P + \frac{\propto}{\beta} P$$

If $\propto = 10$, but also $\beta = 10$, then $F = 2P$. The downward force required to produce a downward displacement ten times as large as the upward displacement is simply twice the magnitude of the upward force, due to the reduced stiffness under downward loading. In Eq. 6, the first term on the right hand side is the same as Eq. 4. In other words, the upward force must first be cancelled out. But the second term, representing the component that overcomes structural stiffness, is reduced by a factor β due to the reduced stiffness under downward loading.

The concept described above is sought to be applied to the airfoil chordwise bending (camber) problem. Figure 1 shows a schematic representation of airfoil camber displacement versus upward/downward force. The line AOB (in red) represents the behavior if the airfoil had a very large chordwise bending stiffness. Under an upward aerodynamic force (operating point A), the upward camber deformation would be very small (point A'), as required, due to the high chordwise bending stiffness. However, assuming that the desired downward camber under actuation is substantially larger, putting the airfoil at operating point B, the required actuation force (point B') is observed to be extremely large due to the high stiffness. Conversely, the line COD (in green) represents the behavior if the airfoil had a very low chordwise bending stiffness. In that case, the desired downward camber displacement (operating point C) could be achieved at a much lower actuation force requirement (point C'). However, the upward camber deformation under aerodynamic load (operating point D) would increase tremendously (point D'). The proposed goal is to operate over the solid portion (OA) of the red curve under upward aerodynamic loads, and over the solid portion (OC) of the green curve at reduced stiffness under downward actuation load. By effectively "bending" the force/displacement curve and operating along COA, the deformation under aerodynamic load remains small (point A'), as does the actuation force to achieve large downward camber (point C' instead of point B'). Similar to the simple cantilever beam example presented earlier, the magnitude of the actuation force required A"OC' comprises of the portion A"O to overcome aerodynamic load and a smaller component OC' (compared to OB') to overcome the reduced chordwise bending stiffness.

Next, the study explores methods for realizing a variable chordwise bending stiffness under upward and downward loading. A NACA 0012 airfoil is chosen for the study, and as shown in Figure 2 it comprises of a rigid leading-edge D-spar extending from the nose to 32.5% chord, followed by a conformable region extending another 42.5% chord, and finally a rigid trailing-edge section over the final 25%. The conformable section comprises of a serial arrangement of vertebrae like elements (based on Ref. 23) along with a compliant skin and enables chordwise bending (camber) deformation at modest force. For the calculations in this study, a concentrated upward or downward force is applied at the point indicated on Figure 2 at the beginning of the rigid trailing-edge section.

The first method considered to achieve the desired difference in stiffness under upward and downward bending loads was to introduce a thick, segmented lower skin (Figure 3) over the conformable section. While the skin is continuous on the outer surface, slits are introduced through the thickness normal to the inner surface as depicted in the figure. In essence, it appears like a number of "blocks" or "bricks" are bonded to the inner surface of the lower skin. When the airfoil cambers downward, the bricks spread open and offer no resistance to deformation. On the other hand, upward camber would result in the blocks coming into contact and drastically increasing the force requirement (and therefore the stiffness). One of the limitations of this method is that the high stiffness does not come into effect till the gaps between the blocks/segments close. So if the manufacturing methods introduce finite gaps between the segments, this will result in a certain upward deformation under aerodynamic loads before the high stiffness comes into effect.

The second method considered was to use a rigid cantilever extending from the rear of the spar adjacent to the camber morphing rib. As shown in Figure 4, the underside of the cantilever is in contact with the lower skin in the undeformed configuration. Under upward aerodynamic load, the lower skin (and outer airfoil shell) pushes firmly against the rigid cantilever which offers a very large resistance (and high stiffness) to upward camber deformation. Conversely, under downward actuation load, the lower skin (and outer airfoil shell) disengages from the rigid cantilever. With the cantilever offering no resistance to downward camber deformation, the stiffness under actuation load is greatly reduced. A decision was made to continue with the rigid cantilever concept and the segmented skin concept was dropped from further consideration for this study due to manufacturability.

A calculation of the deformation of the system under concentrated upward and downward forces was undertaken using the ABAQUS^{TM} Finite Element Analysis software (version 6.13). The leading-edge spar was assumed to be rigid, as was the trailing-edge section. For the conformable section between, the lower skin and the vertebrae (one integral structure) were assumed to be made out of Delrin^{TM} (modulus 450,000 psi), the rigid cantilever was assumed to be made out of Aluminum (modulus $10x10^6$ psi), and the top skin was assumed to have the axial stiffness properties of an elastomer (1,200 psi). The ABAQUS^{TM} model is generated from the Selig point data of a NACA 0012 airfoil, scaled to a chord length of 18 inches. The thickness of the structural elements in the vertebrae, and that of the lower skin, was 1% chord. The majority of the model was automatically seeded with a mesh consisting of 2-D CPS4R 4-node bilinear and CPS3 3-node linear plane strain elements (with reduced integration and hourglass control), while the upper skin was modeled with B21 planar beam elements (with linear interpolation)

and assigned a cross-sectional geometry to facilitate in plane extension while restricting out of plane bending. A total 44,395 nodes is used to model the conformable airfoil rib section (including the vertebrae and skin), while the number of nodes used to model the Aluminum cantilever ranges from 1195 (short cantilever) to 1633 elements (full-length cantilever), and numerical convergence was verified. Figure 5 shows the ABAQUS™ mesh used over a portion of the conformable section. Calculated deformations are obtained under applied (upward and downward) loads. .XFOIL panel method analysis was used to compute the pressure on the airfoil at 0.3 Mach No. and 4 deg angle of attack, and the conversion of the integrated loads over the aft section to an equivalent point force at 75% chord was used to define the range of upward forces (representative of aerodynamic loads) applied on the airfoil. An equivalent camber deformation is calculated as the arctangent of the ratio of the vertical tip deflection to 67.5% chord length (distance from the rear of the leading-edge spar to the trailing-edge). The calculated FE deformations are also used to examine the stresses in the vertebrae and the mean strains in the skins.

III. Finite Element Model Results and Discussion

The length of the rigid cantilever designed to stiffen the system under upward loading was parametrically varied in this study. Attached to the rear of the rigid leading-edge spar at 32.5% chord, and extending along the chord toward the trailing-edge up to 75% chord, the longest cantilever considered extends over the entire conformable region undergoing chordwise bending. Figure 6 shows the airfoil under a downward load, when such a full-length cantilever is used. From the figure it is observed that at some magnitude of camber deflection the upper skin comes in contact with the cantilever, thereby preventing further downward camber deflection. The maximum camber achieved with the full-length cantilever was 10 deg. Figure 7 shows ABAQUS™ simulation results of force versus trailing-edge tip deflection under upward and downward loads. The section of the red line with symbols represents deformation under upward load while the section of the blue line with symbols represents deformation under downward load. Clearly the airfoil is much more compliant under downward deflection, and vice-versa. The stiffness ratio (ratio of the slopes of the portions of the curve under upward and downward loading) is calculated to be 15.43. It should be noted that the in the absence of the cantilever, the displacement under upward load would be represented by the extrapolated section of the blue line without any symbols. The blue line, in general, represents the chordwise bending stiffness of the compliant core (comprising of serially attached vertebrae-like sections) and the upper and lower skin, and the portion without any symbols represents the contribution of the core and skins to the total stiffness under upward deflection. The difference between the red line with symbols, and the blue line without symbols, represents the contribution of the cantilever to stiffness under upward deflection. Extrapolation of the red line to the region without symbols indicates how much larger the required actuation force would be to achieve a desired camber deflection if the stiffness to resist aerodynamic loads was not reduced (by disengagement of the cantilever).

If camber deflections larger than the 10 deg achieved above are required, the length of the cantilever can be reduced. Figure 8 shows the airfoil under a downward load, when a moderate length cantilever (82% of the full-length cantilever) is used. The upper skin still comes in contact with the cantilever but at a much higher camber deflection (19 deg). Figure 9 shows ABAQUS™ simulation results of force versus trailing-edge tip deflection under upward and downward loads for the moderate length cantilever. The section of the red line with symbols once again represents deformation under upward load. The section of the blue line with symbols, representing deformation under downward load, is identical to Figure 7. While the moderate length cantilever allows a larger maximum camber deflection, the stiffness under upward loading is clearly reduced (compare Figure 9 to 7). The stiffness ratio (ratio of the slopes of portions of the curve under upward and downward load) is in this case calculated to be 5.51.

Even larger maximum camber deflections under downward load can be achieved by further reducing the length of the cantilever. Deformation under downward actuation load with the use of a short cantilever (57% of the full-length cantilever) is shown in Figure 10. At a downward camber deflection of 19 deg, the upper skin is not in proximity of (and at risk of contact with) the cantilever. Figure 11 shows ABAQUS™ simulation results of force versus trailing-edge tip deflection under upward and downward loads for the short cantilever. The section of the blue line with symbols, representing deformation under downward load, is identical to Figures 9 and 7. The chordwise bending stiffness under upward load is seen to be further reduced (compare the reduced slope of the red line with symbols in Figure 11 to Figures 9 and 7), and the stiffness ratio (ratio of the slopes of the portions of the curve under upward and downward loading) is in this case of the short cantilever calculated to be 2.33. The short cantilever, while effectively removing maximum camber constraints under downward loading, is less effective in stiffening the system under upward loading.

Figure 12 compares the deformation under upward load with the use of the full-length, moderate-length, and short cantilevers. With the full-length cantilever, the rigid trailing-edge region is seen to essentially pivot about the end of the cantilever. For the moderate-length cantilever, the section of the conformable region aft of the cantilever tip is observed to undergo chordwise bending, and the slope at the end of this conformable region carries into the rigid trailing-edge. For the short cantilever, the region undergoing chordwise bending is significantly increased, as is the upward trailing-edge tip deflection. From the results in Figure 12 the reduction in stiffness under upward load with decreasing cantilever length can be attributed to chordwise bending experienced over an increased length of the conformable region aft of the cantilever tip.

In addition to change in cantilever length, the modulus of elasticity of the cantilever was varied. These comparisons were conducted for the moderate-length cantilever. The baseline cantilever was assumed to be made out of Aluminum (Young's modulus $10x10^6$ psi). ABAQUS™ simulation results were obtained for a reduced modulus of $5x10^6$ psi, and with the modulus increased to $20x10^6$ psi. The change in stiffness ratio (ratio of the slopes of the portions of the curve under upward and downward loading) with change in cantilever modulus is presented in Table 1. Clearly, change in cantilever modulus has a relatively small influence on stiffness ratio, relative to change in cantilever length.

Figures 13 and 14, respectively, show the stress distribution in the vertebrae in the conformable section of the airfoil and the strain distribution in the upper skin, corresponding to a 10 deg downward camber deflection. Regions of high stress concentration are observed at the junctions between successive vertebrae in Figure 13. If the rib was fabricated out of Aluminum, the allowable material limits would be reached at a downward camber deformation of about 4 deg. For a rib fabricated out of Delrin™, a 12.5 deg downward camber deflection can be realized before allowable material limits are reached. Of course, structural design modifications to the compliant core could be introduced to achieve the desired camber deformation without violating constraints on the allowable material limits. Indicated on Figure 14 is the mean strain in segments of the upper skin over individual vertebrae sections. The strain, mostly uniform over a single vertebrae, is highest over the second vertebrae reaching a mean value of 2.3% corresponding to a 10 deg downward camber. The strain levels in the skin play an important role in skin material selection. The strains in any skin segment is related to the relative rotation between adjacent vertebrae, with greater relative rotation leading to larger strains in the skin segment between. The maximum skin strains can be reduced by limiting the relative rotation between successive vertebrae through structural optimization, while still realizing a specified camber deformation. In the current study, the vertebrae design is completely *ad hoc*, with no effort directed to reduction in maximum skin strains or stress concentrations at the vertebrae junctions.

IV. Prototype Design, Fabrication, and Assembly

To experimentally verify that the proposed design can produce differences in stiffness under upward and downward camber loads, a CAD model is generated followed by the fabrication of components for prototype assembly (see Figure 15). Two 18 inch chord, 0.5 inch width NACA 0012 rib sections are designed and fabricated out of Delrin™ using a waterjet cutter. The ribs are to be bolted at either end of a 11 inch wide, 2.1875 inch tall and 1 inch thick block of Aluminum which will represents the aft of the spar of a 12 inch spanwise section of helicopter rotor blade, or wing. The figure shows four rigid Aluminum cantilever members, each of length 6.375 inches, maximum height of 0.875 inches and a width of 0.5 inches, to be bolted to the aft of the Aluminum spar. The length of the cantilever sections corresponds to the moderate-length cantilever extending over 82% of the conformable region, discussed in the previous section. A 1 ft x 1 ft flat lower skin , made of Delrin™, is to be bolted to the underside of the ribs and the Aluminum block representing the aft of the spar over the section between the ribs. Bolting it as such sets the Delrin™ skin flush against the underside of the Aluminum cantilevers. Therefore, any upward displacement of the lower skin will impinge upon the cantilevers, whereas downward motion is unimpeded by the cantilevers. A trailing-edge section (not shown in the hardware arrangement) will comprise of an Aluminum rod running along the span of the section and bolted to each of the ribs in the aft region. The Aluminum rod will be used to apply upward and downward loads, which are expected to transmit equally to each of the two ribs.

After assembly, the overall system will be mounted such that the spar region is clamped to the edge of a table while the aft region overhangs. A downward load will be applied by suspending weights at the center of the trailing edge Aluminum rod, and the corresponding tip displacements will be measured. An upward load will effectively be applied by simply reversing the prototype (rotating upside-down) and, once again, suspending weights. The force

versus displacement data obtained through experiment and the calculated stiffness will be used to validate the ABAQUS™ finite element simulation results.

V. Summary and Concluding Remarks

Aerodynamic loads on an airfoil (suction on the upper surface and pressure on the lower surface) tend to camber the region aft of the spar upward. In many applications, downward camber deflections are sought for high-lift or load redistribution. This paper focuses on the design of the aft section of an airfoil that is very stiff under upward loading but much more compliant under downward loading, so that the deformation under aerodynamic loading is very small but the actuation force requirement to camber downward is modest, as well. The design utilizes a rigid cantilever extending from the rear of the spar toward the trailing-edge, and flush with the lower skin of the airfoil. Under upward load (representative of aerodynamic pressure) the rigid cantilever engages and its added stiffness inhibits upward camber deformation. But under downward load (representative of an actuated state), the lower skin breaks contact with the cantilever, and camber deformation can be achieved at low actuation effort. ABAQUS™ finite element simulations were conducted for a variable camber NACA 0012 airfoil. From the simulation results the following conclusions were drawn:

1. For a "full-length" cantilever extending over the entire length of the conformable section (between the leading-edge D-spar and the trailing-edge section), the effective stiffness under upward loading was calculated to be 15.43 times the stiffness under downward loading, but the maximum downward camber deformation was limited to 10 deg due to contact between the cantilever and the upper skin.
2. A "moderate-length" cantilever extending over 82% of the length of the conformable section allows a larger maximum camber deformation (19 deg) but the stiffness under upward load is reduced (ratio of stiffness under upward load to the stiffness under downward load is reduced to 5.51).
3. A "short" cantilever cantilever extending over 57% of the length of the conformable section effectively eliminates any constraint on camber deformation, but the stiffness under upward load is further reduced (with the stiffness ratio down to 2.33).
4. Reduction in effective stiffness under upward load with reduced cantilever length is attributed to bending deformation over the portion of the conformable section between the cantilever tip and the beginning of the trailing-edge section.
5. Change in cantilever modulus has a smaller effect on the stiffness ratio than change in cantilever length. Using a moderate-length cantilever, reducing the modulus to half that of Aluminum reduces the stiffness ratio from 5.51 to 5.30, while increasing the modulus to double that of Aluminum increases the stiffness ratio from to 5.60.

References

1. Hall, J. 1989. ''Executive Summary AFTI/F-111 Mission Adaptive Wing'', Technical Report, WRDC-TR-89-2083 Wright Research Development Center, Wright_Patterson Air Force Base.
2. Pendleton, E.W., Bessette, D., Field, P.B., Miller, G.D. and Griffin, K.E. 2000. ''Active Aeroelastic Wing Flight Research Program: Technical Program and Model Analytical Development,'' *Journal of Aircraft,* 37:554-561.
3. Kudva, J. 2004. ''Overview of the DARPA Smart Wing Project,*''Journal of Intelligent Material Systems and Structures,*15: 261-267.
4. Bartley-Cho, J.D., Wang, D.P., Martin, C.A., Kudva, J.N. and West, M.N. 2004. ''Development of High-rate, Adaptive Trailing Edge Control Surface for the Smart Wing Phase 2 Wind Tunnel Model,'' *Journal of Intelligent Material Systems and Structures*, 15:279-291.
5. Nguyen, N., and Urnes, J., Sr., "Aeroelastic Modeling of Elastically Shaped Aircraft Concept Via Wing Shaping Control for Drag Reduction," AIAA Atmospheric Flight Mechanics Conference 13 - 16 August 2012, Minneapolis, Minnesota, AIAA 2012-4642.
6. Strelec, J. K., Lagoudas, D. C., Khan, M. A., and Yen, J., "Design and Implementation of a Shape Memory Alloy Actuated Reconfigurable Airfoil," *Journal of Intelligent Material Systems and Structures* 2003, 14: 257, DOI: 10.1177/1045389X03034687
7. Barbarino, S., Pecora, R., Lecce, L., Concilio, A., Ameduri, S., De Rosa, L., "Airfoil Structural Morphing Based on S.M.A. Actuator Series: Numerical and Experimental Studies." *Journal of Intelligent Material Systems and Structures*, Jul 2011; vol. 22: pp. 987-1004.

8. Pecora, R., Barbarino, S., Concilio, A., Lecce, L., Russo, S., "Design and Functional Test of a Morphing High-Lift Device for a Regional Aircraft." *Journal of Intelligent Material Systems and Structures*, Jul 2011; vol. 22: pp. 1005-1023.
9. Ameduri, Salvatore, Brindisi, Angela, Tiseo, Barbara, Concilio, Antonio, Pecora, Rosario, "Optimization and integration of shape memory alloy (SMA)-based elastic actuators within a morphing flap architecture." *Journal of Intelligent Material Systems and Structures*, Mar 2012; vol. 23: pp. 381-396.
10. Bil, Cees, Massey, Kevin, Abdullah, Ermira J, "Wing morphing control with shape memory alloy actuators." *Journal of Intelligent Material Systems and Structures*, May 2013; vol. 24: pp. 879-898.
11. Anusonti-Inthra, P., R. Sarjeant, M. Frecker, and F. Gandhi (August 2005) "Design of a Conformable Rotor Airfoil Using Distributed Piezoelectric Actuators," *AIAA Journal*, 43, No. 8, pp. 1684–1695.
12. Gandhi F, Frecker M and Nissly A (2008) Design optimization of a controllable camber rotor airfoil. *AIAA Journal*, 46(1): 142–153.
13. Grohmann B, Maucher C, Prunhuber T, et al. (2008) Multidisciplinary design and optimization of active trailing edge for smart helicopter rotor blade. *Mechanics of Advanced Materials and Structures* 15(3): 307–324
14. Bilgen, O., Kevin B Kochersberger, Daniel J Inman and Osgar J Ohanian III, "Macro-Fiber Composite actuated simply supported thin airfoils." 2010 *Smart Mater. Struct.* 19 055010 doi:10.1088/0964-1726/19/5/055010
15. Bilgen, O., Kevin B. Kochersberger, Daniel J. Inman, and Osgar J. Ohanian "Novel, Bidirectional, Variable-Camber Airfoil via Macro-Fiber Composite Actuators." *Journal of Aircraft* 2010 47:1, 303-314.
16. Bernhammer, Lars O, Teeuwen, Sjors PW, De Breuker, Roeland, van der Veen, Gijs J, van Solingen, Edwin, "Gust load alleviation of an unmanned aerial vehicle wing using variable camber." *Journal of Intelligent Material Systems and Structures*, May 2014; vol. 25: pp. 795-805.
17. Woods, B. K. S., Friswell, M., and Wereley, N., "Advanced Kinematic Tailoring for Morphing Aircraft Actuation," *AIAA Journal*, Vol. 52, No. 4, April 2014, DOI: 10.2514/1.J052808.
18. Yokozeki, T., Aya Sugiura, and Yoshiyasu Hirano, "Development of Variable Camber Morphing Airfoil Using Corrugated Structure." Journal of Aircraft, http://dx.doi.org/10.2514/1.C032573.
19. Ursache, N.M., Andy J. Keane, and Neil W. Bressloff, "Design of Postbuckled Spinal Structures for Airfoil Camber and Shape Control." AIAA Journal 2006 44:12, 3115-3124.
20. Mistry, M., and Gandhi, F., "Design, fabrication and benchtop testing of a helicopter rotor blade section with warp-induced spanwise camber variation," *Proceedings of the 69th American Helicopter Society Annual Forum*, Phoenix, AZ, May 21-23 2013.
21. Campanile, L.F. and Sachau, D. 2000. ''The Belt-rib Concept: A Structronic Approach to Variable Camber,'' Journal of Intelligent Material Systems and Structures, 11:215-224.
22. Campanile, L.F., Keimer, R. and Breitbach, E.J. 2004. ''The 'Fishmouth' Actuator: Design Issues and Test Results,'' Journal of Intelligent Material Systems and Structures, 15: 711-719.
23. Gandhi, F., and Anusonti-Inthra, P., "Skin Design Studies for Variable Camber Morphing Airfoils," *Smart Materials and Structures*, Vol. 17, No. 1, Feb. 2008.
24. Olympio, K. R., and Gandhi, F., "Flexible Skins for Morphing Aircraft using Cellular Honeycomb Cores," *Journal of Intelligent Material Systems and Structures*, Vol. 21 (17), November 2010, pp. 1719-1735, doi:10.1177/1045389X09350331.
25. Olympio, K. R., and Gandhi, F., "Zero-Poisson's Ratio Cellular Honeycombs for Flexskins Undergoing One-Dimensional Morphing," *Journal of Intelligent Material Systems and Structures*, Vol. 21 (17), November 2010, pp. 1737-1753, doi:10.1177/1045389X09355664.
26. Olympio, K. R., Gandhi, F., Asheghian, L., and Kudva, J., "Design of a Flexible Skin for a Shear Morphing Wing," *Journal of Intelligent Material Systems and Structures*, Vol. 21 (17), November 2010, pp. 1755-1770, doi:10.1177/1045389X10382586.
27. Murray, G., Gandhi, F., and Bakis, C., "Flexible Matrix Composite Skins for One-Dimensional Wing Morphing," *Journal of Intelligent Material Systems and Structures*, Vol. 21 (17), November 2010, pp. 1771-1781, doi:10.1177/1045389X10369719.
28. Thill, C., Etches, J., Bond, I., Potter K., and Weaver, P., "Morphing skins," *The Aeronautical Journal*, Vol. 112, No. 1129, March 2008.

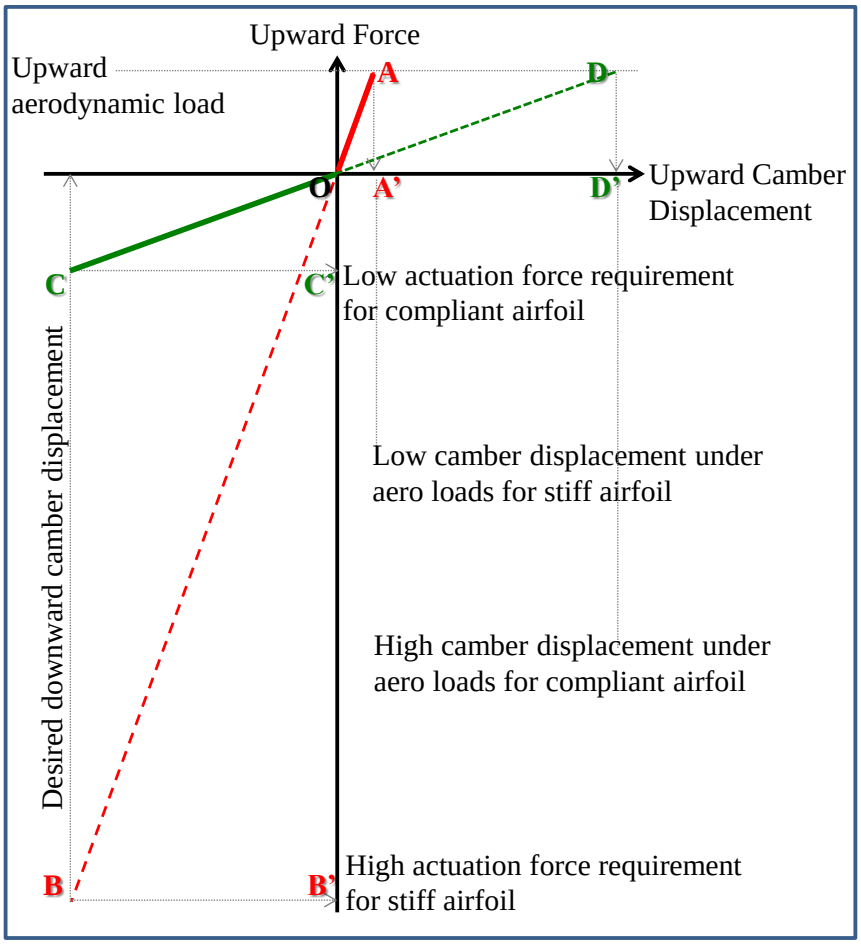

Figure 1: Schematic representation of airfoil camber displacement versus upward/downward force

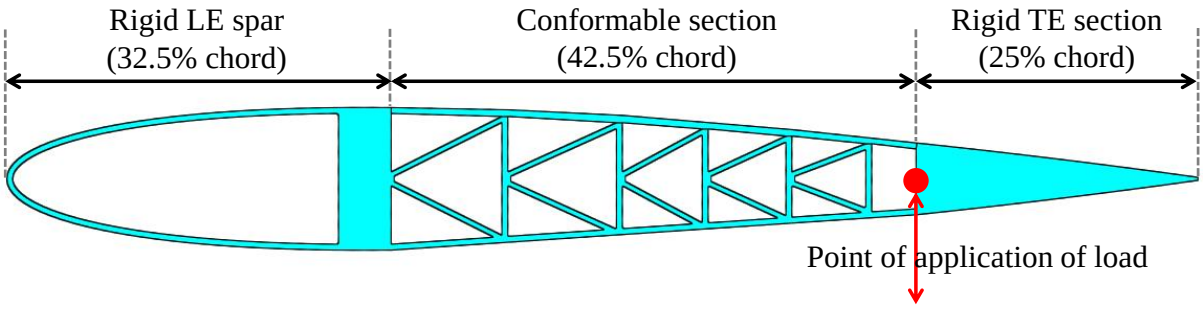

Figure 2: Camber morphing variant of a NACA 0012 airfoil used for simulations in this study

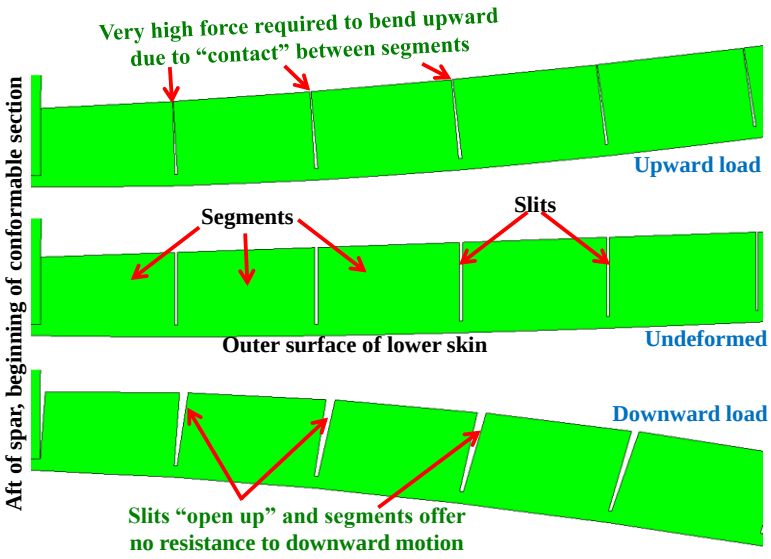

Figure 3: Thick segmented lower surface skin over the conformable section, in various loading states

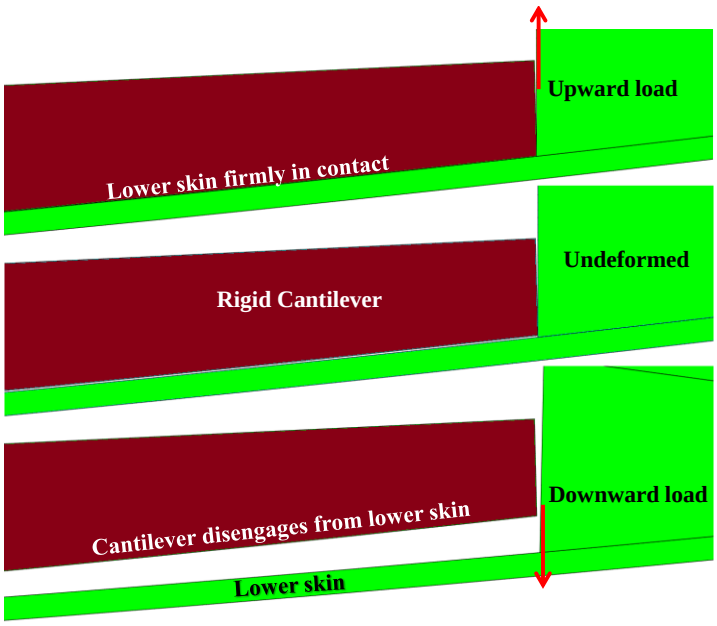

Figure 4: Rigid cantilever and lower surface skin, in various loading states

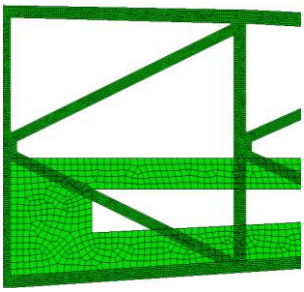

Figure 5: ABAQUS^{TM} mesh used over a portion of the conformable section

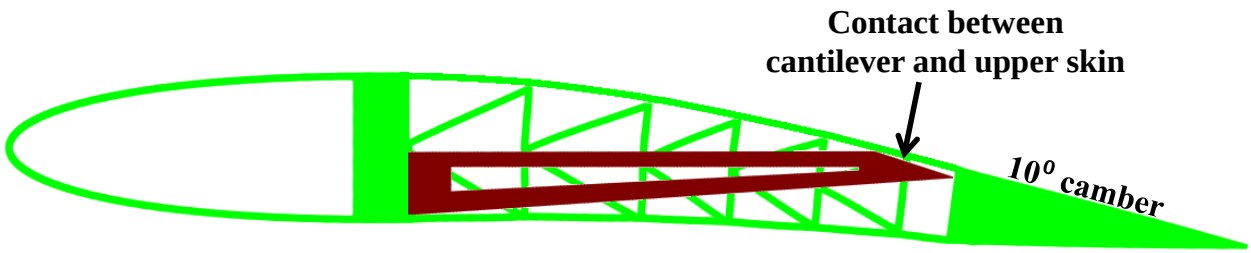

Figure 6: Airfoil with full-length cantilever under a downward load

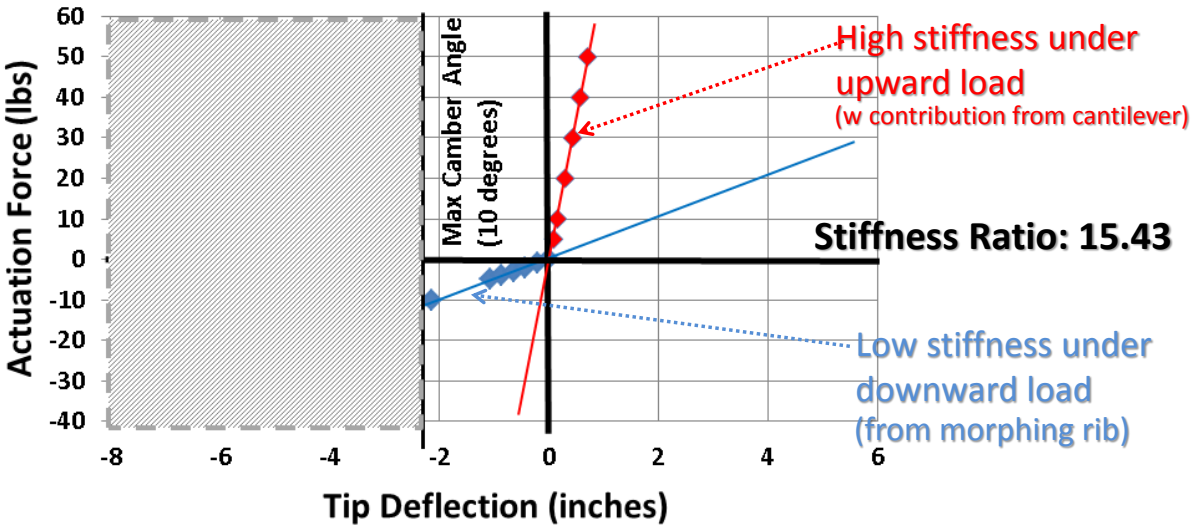

Figure 7: ABAQUS™ force versus tip deflection simulation results with full-length cantilever

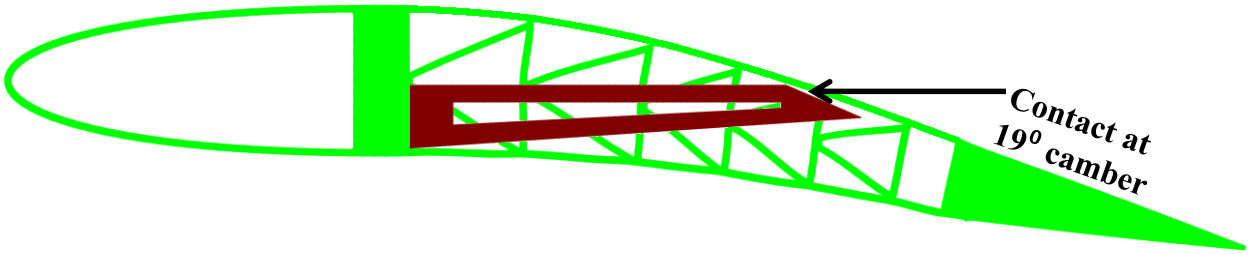

Figure 8: Airfoil with moderate-length cantilever under a downward load

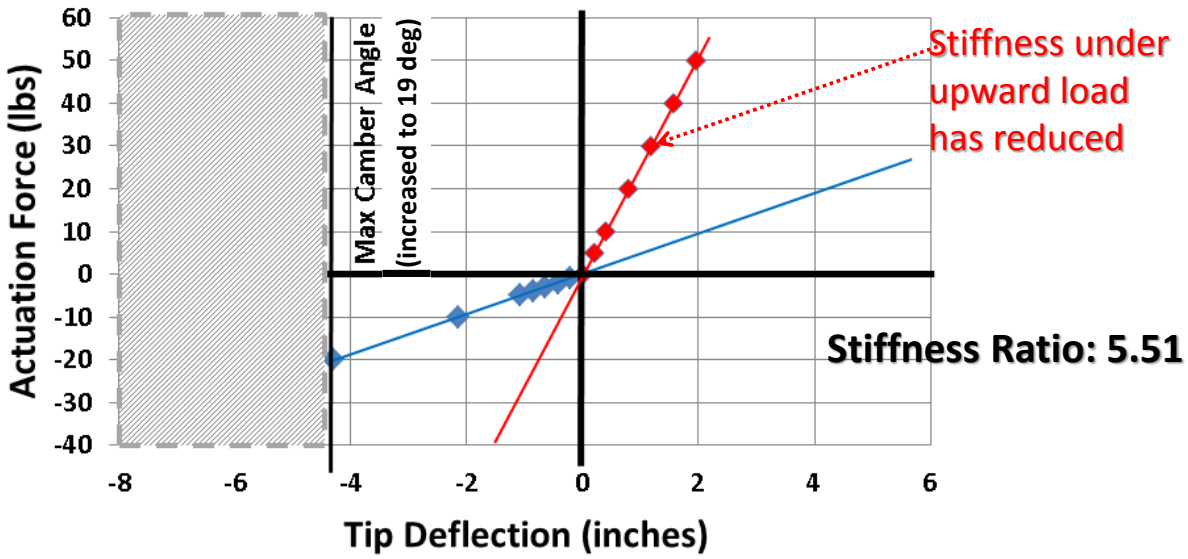

Figure 9: ABAQUS™ force versus tip deflection simulation results with moderate-length cantilever

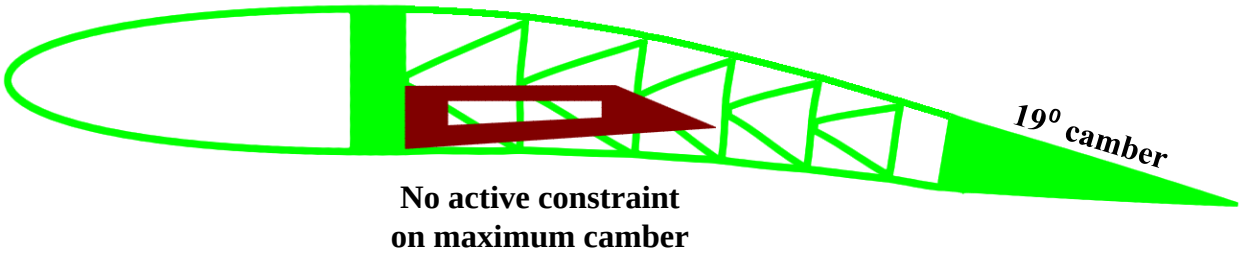

Figure 10: Airfoil with short cantilever under a downward load

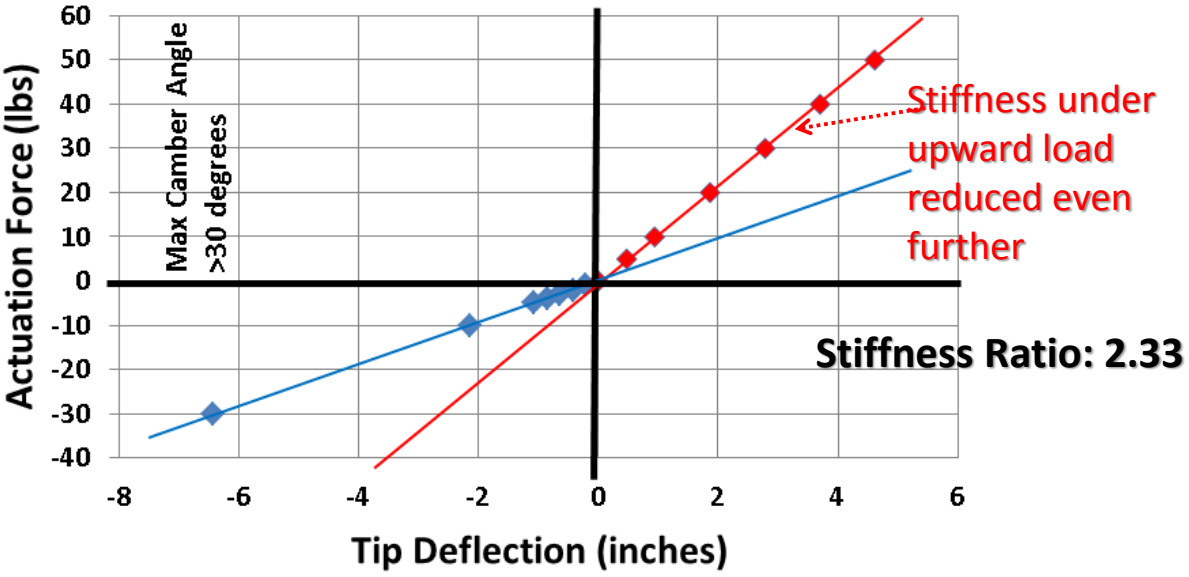

Figure 11: ABAQUS™ force versus tip deflection simulation results with short cantilever

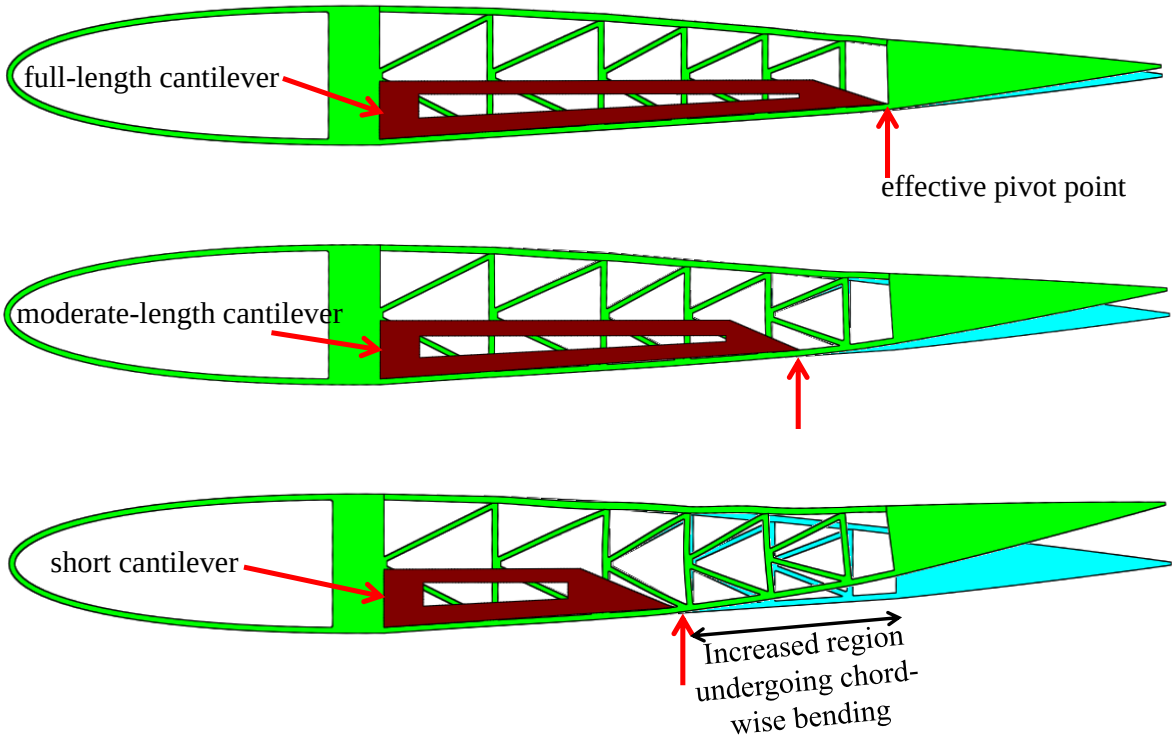

Figure 12: Deformation under upward load with the use of the full-length, moderate-length, and short cantilevers

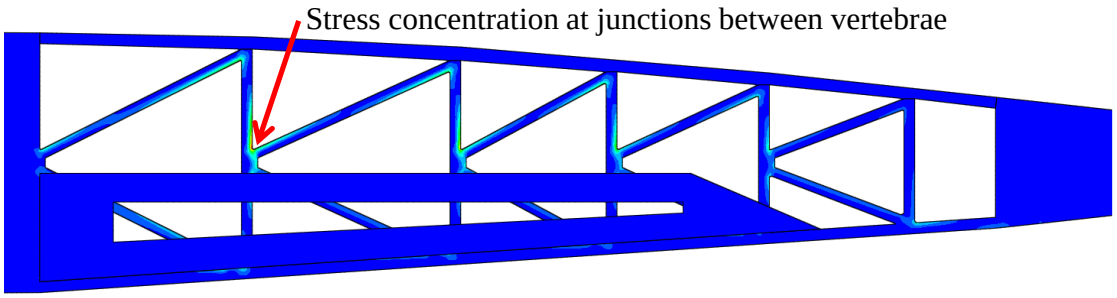

Figure 13: Stress distribution in vertebrae in the conformable section for 10 deg downward camber deflection

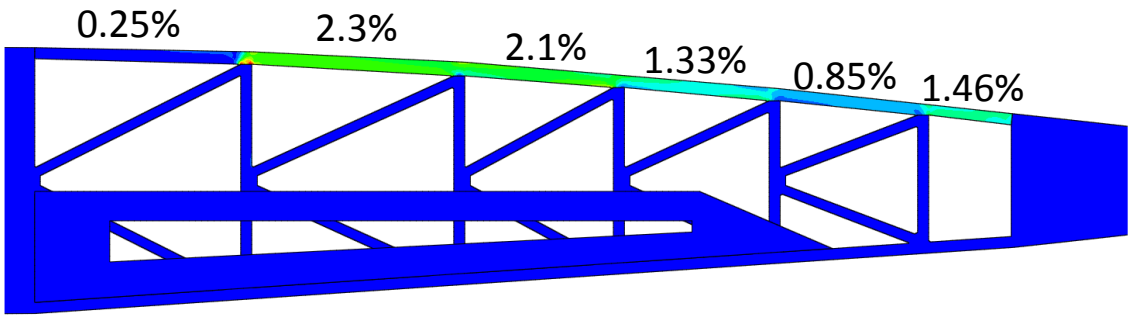

Figure 14: Strain distribution in upper skin in the conformable section for 10 deg downward camber deflection

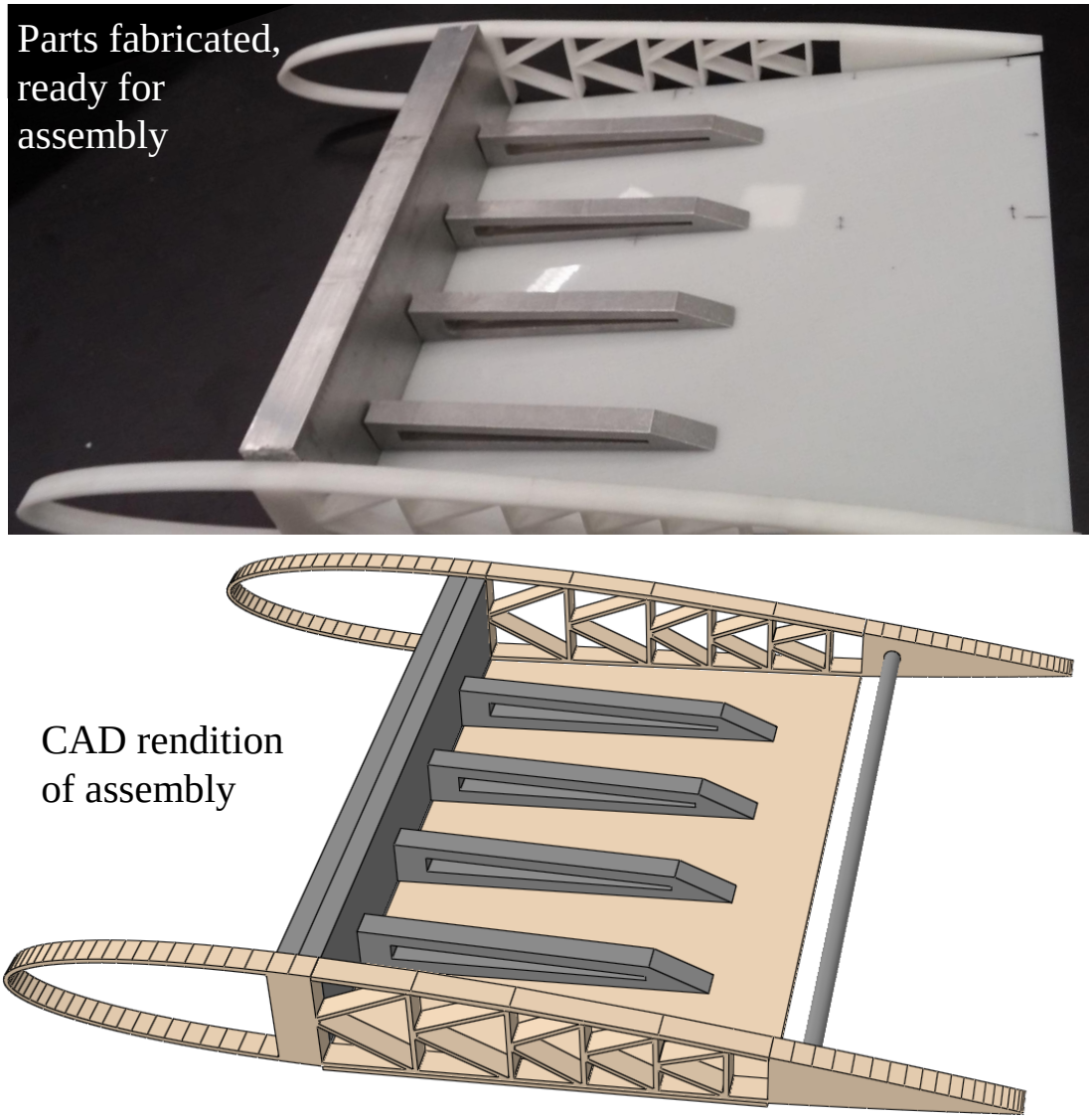

Figure 15: CAD model of prototype and components fabricated for assembly

Cantilever Modulus	Stiffness Ratio
$5x10^6$ psi	5.30
$10x10^6$ psi (Aluminum)	5.51
$20x10^6$ psi	5.60

Table 1: Change in stiffness ratio with change in cantilever modulus